

Investigating the Electrical Properties of Monolayer and Bilayer h-BNs via Atomic Force Microscopy

Nan Wang, Yiding Song, Li Wang, Kaihui Liu, and Ya Yang*

Hexagonal boron nitride (h-BN) is one of the most important 2D materials which attracts tremendous attention for the demonstrated great potential applications in optical and electronic devices. However, whether there are significant differences in the electrical properties of h-BN with different layers and its mechanism is not revealed clearly. Based on the atomic force microscopy (AFM) technology, the electrical properties of monolayer h-BN and bilayer h-BN are investigated. It is found that bilayer h-BN shows quite different electrical characteristics from monolayer h-BN. It is proposed that the difference of work functions between monolayer h-BN and bilayer h-BN contributes to the different electrical characteristics. Meanwhile, the interlayer coupling resistance due to coupling between the layers of h-BN also plays a vital role in electron transport. Besides, the effect of load force on electrical characteristics of h-BN with different layers is also investigated. This work provides a new insight to understand the effect of the different layers on electrical properties of h-BN. It is hoped that this valuable experimental data can offer meaningful suggestions for future studies and applications on h-BN and other 2D nanomaterials in general.

1. Introduction

2D materials with ultrathin nature such as transition metal dichalcogenides (MoS₂, MoSe₂, WS₂) or black phosphorus have drawn considerable attention. They have been investigated for their great potential in electronic devices with new functions and photocatalyst, because they can meet the requirements of the device for being more diminutive, super-speedy, and multifunctional. And, one of the most important 2D nanomaterials is hexagonal boron nitride (h-BN), which is so-called white graphene, owing to the analogue structure of graphene. H-BN has many unique properties, for instance, large optical bandgap (5.8 eV),^[1,2] excellent mechanical strength, good chemical inertness, and high thermal conductivity even at severe temperatures.^[3,4] Many studies have been carried out to study the relation between the unique structure

and properties of h-BN.^[5–8] Moreover, the unique structure and properties have promoted their use in various applications in the field of the dry-lubricant, deep ultraviolet emitter, and gate-insulating materials.^[1,9,10] The most promising application of the h-BN layer is to be used as substrates such as, growth templates,^[11,12] and tunneling barriers,^[13–16] because of its atomic flatness and good insulation. For example, an h-BN layer with a modified dielectric interface was realized to improve carrier transport and heat spreading of a WSe₂ field-effect transistor.^[15]

However, the size of h-BN single crystals which are no more than one millimeter^[16,17–21] in most cases, due to difficulties in the growth of crystals, has limited their applications for 2D materials devices that are dependent on large, high-quality single crystals. Wang et al. has achieved a high-quality h-BN sample on a Cu (110) vicinal surface.^[22] It was confirmed that the as-grown sample was a single-crystal h-BN monolayer with a size as large as 100 cm². Furthermore, on many of the large single-crystal h-BN monolayers, a small bilayer h-BN was also observed. It has been reported that the characteristics of many 2D materials are affected by the number of layers.^[23–25] In terms of mechanical properties, it has been established that the mechanical strength of BN nanosheets was insensitive when the thickness was added.^[26] Moreover, some previous work has investigated the electronic properties of h-BN according to the number of layers. However, most of them focus on the electronic properties of BN as an insulating layer for other

Dr. N. Wang, Y. Song, Prof. Y. Yang
CAS Center for Excellence in Nanoscience
Beijing Key Laboratory of Micro-Nano Energy and Sensor
Beijing Institute of Nanoenergy and Nanosystems
Chinese Academy of Sciences
Beijing 101400, P. R. China
E-mail: yayang@binn.cas.cn

Dr. N. Wang, Y. Song, Prof. Y. Yang
School of Nanoscience and Technology
University of Chinese Academy of Sciences
Beijing 100049, P. R. China

Prof. L. Wang
Beijing National Laboratory for Condensed Matter Physics
Institute of Physics
Chinese Academy of Sciences
Beijing 100190, China

Prof. K. Liu
State Key Laboratory for Mesoscopic Physics
Frontiers Science Center for Nano-optoelectronics
School of Physics
Peking University
Beijing 100871, China

Prof. Y. Yang
Center of Nanoenergy Research
School of Physical Science and Technology
Guangxi University
Nanning 530004, P. R. China

 The ORCID identification number(s) for the author(s) of this article can be found under <https://doi.org/10.1002/admi.202100447>.

DOI: 10.1002/admi.202100447

conductive materials.^[27,28] In addition, whether there are significant differences in the electrical properties of h-BN with different layers and its mechanism has not been fully clarified.

Here, benefitting from the high-quality h-BN sample supported by Wang et.al, we investigated the different electrical properties of monolayer h-BN and bilayer h-BN based on the conductive atomic force microscope (C-AFM) technology. We found that bilayer h-BN showed quite different electrical characteristics from monolayer h-BN. This work was focused to investigate the mechanism that makes the difference of electrical characteristics between monolayer h-BN and bilayer h-BN. We proposed that the difference of work functions between monolayer h-BN and bilayer h-BN contributed to the differentiation in electrical characteristics. Meanwhile, the interlayer coupling resistance due to coupling between the h-BN layers also made a great effect on the electron transport.^[29] Then, the effect of load force on the electric conductivity of monolayer h-BN and bilayer h-BN was also investigated. It was found that the monolayer h-BN showed much more sensitivity to the load force than bilayer h-BN. This work offered very significant experimental data and a new perspective to understand the role of the number of layers played on electrical characteristics of h-BN, and further provided a new pathway to tune electrical properties of h-BN-based multifunctional nano-electronics devices.

2. Results and Discussion

A schematic illustration showing the experimental process was showed in **Figure 1a**. When the Pt/Ir-coated silicon AFM tip slid on the surface of h-BN, an external bias was applied from the sample side, and the tip was connected to the ground through an external circuit. Thus, the electrons could be transferred between AFM tip and h-BN film, so current mapping and topographic mapping with high-resolutions were obtained simultaneously. As can be seen from the optical microscopy image (Figure S1, Supporting Information), most of the h-BN grown on the Cu (110) surface showed a triangle shape. It also can be seen that there was a small triangular h-BN (bilayer h-BN) on most of these monolayers h-BN. The AFM topographic mapping (Figure 1c₁) and scanning electron microscopy (SEM) mapping (Figure 1b) displayed the detailed information of the h-BN film. As shown in those images, a bilayer h-BN (white square in Figure 1b₂ and olive square in Figure 1c₂) grew on the monolayer h-BN. The size of the triangular monolayer h-BN was 30–50 μm, while it was ≈5 μm for bilayer h-BN. Figure 1c₂ depicted the cross-sectional height trace of the h-BN corresponding to the blue line on topographic mapping (Figure 1c₁). As illustrated by the height trace, the altitude intercept of the monolayer h-BN and bilayer h-BN was ≈2–3 nm, (Figure 1c₂; Figure S2, Supporting Information). The height of the BN was higher than the thickness of monolayer BN reported by previous work and the noise was also relatively high. It was mainly to ensure the experimental conditions for in situ measurements, the topographic mapping was obtained directly on Cu foils substrate. Generally, Cu foil is not suitable as a substrate for AFM measurement. Because, the surface is not atomically flat, and Cu foil would immediately form an oxide layer in the

air. These factors will cause the measured results to have a large deviation or even a difference of several times. However, in order to measure the electrical properties of h-BN, we need to test on the Cu substrate which can provide a good conductivity.

Multiple *I*–*V* curves (nine data points marked in Figure 1c₁) for monolayer and bilayer h-BN were presented in Figure 1d.e. *I*–*V* curves showed that a Schottky contact was formed across the tip and h-BN interface. Meanwhile, the *I*–*V* curves also exhibited a striking difference of electrical characteristics between monolayer h-BN and bilayer h-BN. First, bilayer h-BN showed much stronger insulation. Under the same test conditions, (an external voltage of ≈ ±1.3 V, and an applied load force of ≈110 nN) the current measured for monolayer h-BN was three orders of magnitude higher than that obtained for bilayer h-BN. For example, when the external bias voltage reached –1 V, the current value of the single-layer BN had reached the threshold value of –500 nA which can be measured by the equipment, while the current of the double-layer BN under the same bias voltage was only ≈ –0.1 nA. Second, although both h-BN with monolayer and bilayer exhibited diode features, bilayer h-BN showed more obvious rectification characteristic. It was much easier to conduct when a negative voltage was applied for bilayer h-BN. As for the monolayer h-BN, compared to the positive voltage, it was also easier to conduct under negative voltage, but with not too much difference.

To understand the discrepant behavior of electrical characteristics between monolayer h-BN and bilayer h-BN, C-AFM was used to measure the current mapping that can show the current distribution of the whole h-BN samples. And the corresponding work functions of the h-BN were also obtained by an interleave scan mode (kelvin probe force microscopy, KPFM). As illustrated in C-AFM current mappings (**Figure 2a**), regardless of whether a negative or positive bias was applied, the bilayer h-BN can show better insulation performance. The corresponding potential mapping (Figure 2b) which value presented the difference value of work functions between the h-BN and tip (i.e., $W_{\text{Potential}} = W_{\text{sample}} - W_{\text{tip}}$), can characterize the work function difference of monolayer and bilayer h-BN. As displayed, we can see that the zone of monolayer h-BN exhibited positive potential while bilayer h-BN exhibited negative potential which indicated that $W_{\text{monolayer}} > W_{\text{tip}} > W_{\text{bilayer}}$. This phenomenon was not just a case. It was discovered in many different h-BN samples (Figure S2, Supporting Information). The cross-sectional line profiles of the images in Figure 2a,b (marked with olive lines) suggested that the tip has a lower work function ≈20 mV than that for monolayer h-BN, but was ≈25 mV higher than that for bilayer h-BN. Therefore, it can be calculated that the work function of single-layer h-BN was ≈45 mV higher than that of double-layer h-BN. And it was closely relevant to the current distribution in current mappings (Figure 2a). Approximately 2 nA current was observed in the monolayer h-BN region while almost no current was observed in the bilayer region. The close correlation suggested that the difference of work functions between monolayer h-BN layer and bilayer h-BN contributed to the different electric conductivity of h-BN. An energy band diagram (Figure 2d,f) of the electronic transmission process was proposed to explain the mechanism. Due to $W_{\text{monolayer}} > W_{\text{tip}}$, the AFM tip had a higher Fermi level than that of monolayer h-BN. When the monolayer

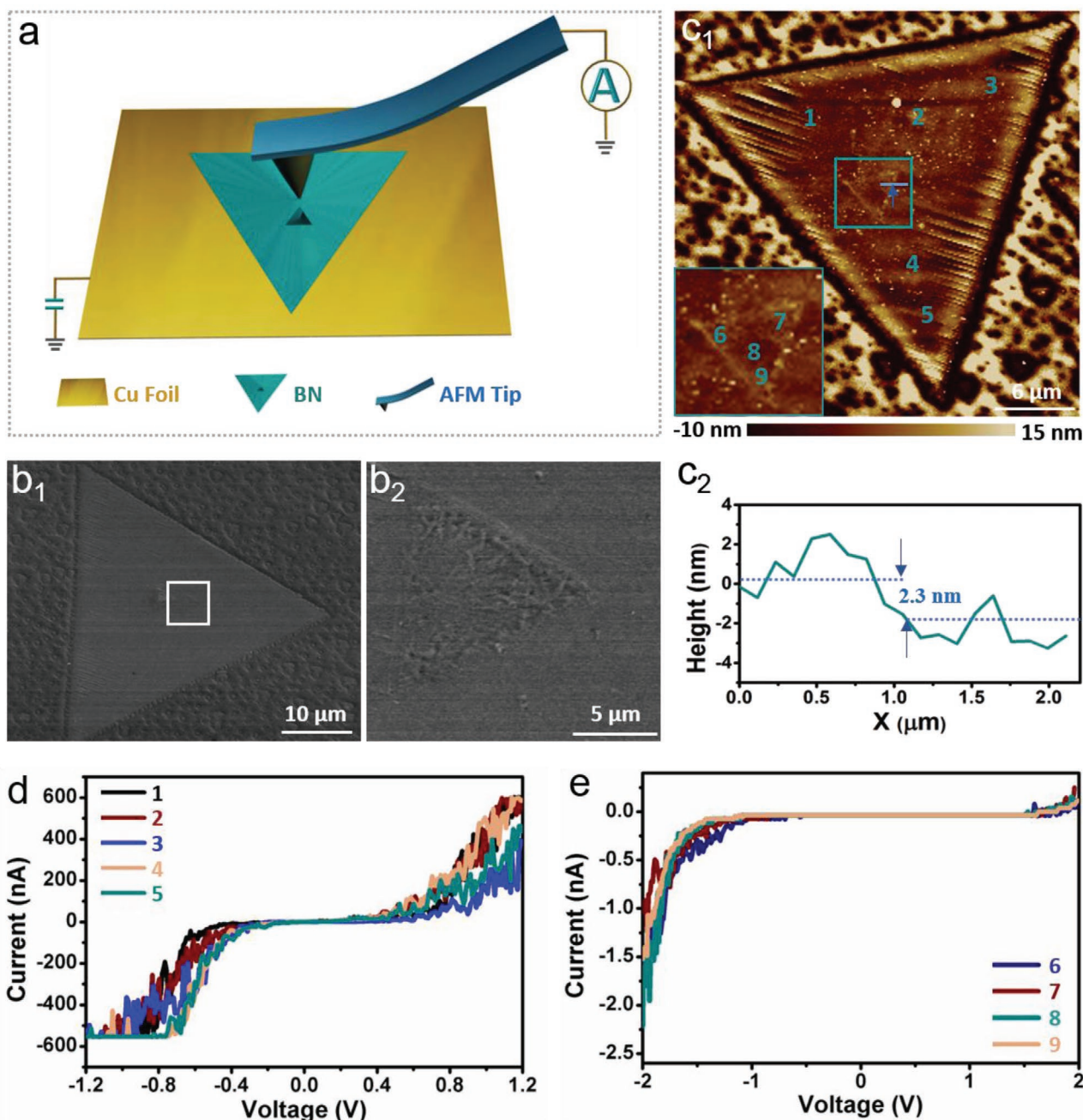


Figure 1. Measurement method, characterization of h-BN, and I - V curves. a) Schematic illustration displaying the experimental process of C-AFM measurement. b₁) Image of an h-BN sample by SEM. b₂) SEM image of bilayer h-BN circled in the white square in Figure 1b₁. c) The AFM topographic mapping (c₁), and the inset image is the topographic mapping of bilayer h-BN zone circled in the olive square, and the cross-section of height trace of the h-BN corresponding to the blue line on topographic mapping (c₂). d) I - V curves for monolayer h-BN (1–5 data points marked on Figure 1c₁) under the load force of 110 nN. e) I - V curves for bilayer h-BN (6–9 data points marked on inset image in Figure 1c₁) under the load force of 110 nN.

h-BN was brought into intimate contact with the tip, as the Fermi levels had to be aligned, the energy bands would bend downward (Figure 2d). Because the external bias was applied to the end of h-BN, when a negative voltage was applied, electrons could transfer from the monolayer h-BN to the tip easily. While, under a positive voltage, electrons transferred from the tip to the monolayer h-BN will encounter a Schottky barrier ($q\psi_1$), which made it tough to conduct. In the case of bilayer h-BN,

the AFM tip had a lower Fermi level than the Fermi level of the bilayer h-BN (Figure 2f). When the bilayer h-BN was brought into intimate contact with the tip, the energy bands had to be upward which caused a higher Schottky barrier ($q\psi_2$). The higher Schottky barrier made it much harder for electron to transfer from the tip to bilayer h-BN. That could explain why the bilayer h-BN exhibited more obvious rectification characteristic than monolayer h-BN.

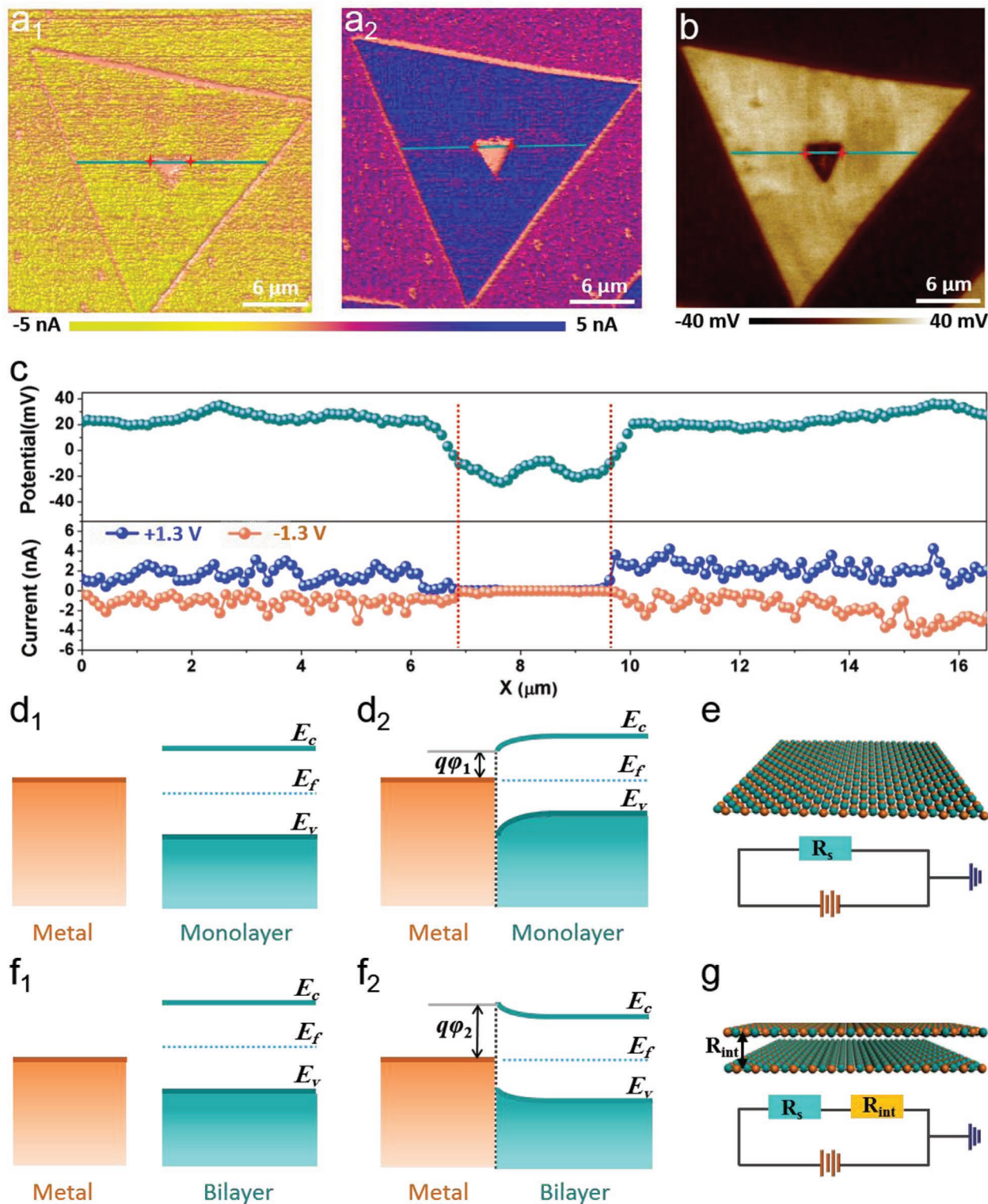


Figure 2. Mechanisms of the different behavior of electrical characteristics between monolayer h-BN and bilayer h-BN. a) C-AFM current mappings when a₁) a negative and a₂) positive external bias was applied. b) Corresponding potential mapping of h-BN. c) Corresponding line-scan profile of potential mapping in Figure 2b and current mappings in Figure 2a. The data between the red parallel lines correspond to the positions between the two red stars in Figure 2a,b. d) Energy band diagram of the working process of monolayer h-BN: d₁) before contact state and d₂) after contact state. e) The equivalent circuit diagram of monolayer h-BN only including Schottky barrier contact resistance. f) Energy band diagram of the electronic transmission process of bilayer h-BN: f₁) before contact state and f₂) after contact state. g) The equivalent circuit diagram of bilayer h-BN, where interlayer resistance (R_{int}) due to the coupling between the h-BN layers made great effect on the total resistance.

However, it still cannot explain all the different behaviors of electrical characteristics between monolayer and bilayer h-BN. First, the Schottky barrier in the level of mV was not enough to make so obvious a difference. Second, it cannot explain why bilayer h-BN can exhibit such an excellent electrical insulation. In prior reports, the lack of sufficient screening of the substrate interface, and the interlayer coupling resistances were thought to be the cause of the dependence of intrinsic properties on the number of layers in many 2D materials.^[30–33] Moreover, a resistor network model was proposed to depict the coupling between graphene layers involving the influence of interlayer screening.^[34] Inspired by these works, and based on the experimental findings, we proposed that the interlayer coupling resistances played an important role in excellent electrical insulation of bilayer h-BN. As illustrated in Figure 2e, in the equivalent circuit diagram of monolayer h-BN, there was only Schottky barrier contact resistance (R_s) that impacted the electron transport. And in the equivalent circuit diagram of bilayer h-BN, the total resistance (R_{total}) contained contributions from the R_s and the interlayer coupling resistance (R_{int}) between the layers as shown in Figure 2g. Moreover, compared to the R_s , the R_{int} may make more impact on the electron transport. Besides, in the process of preparation of h-BN, some defects will form. These defects have been demonstrated to make effects on the electronic, magnetic properties, and chemical reactivity of h-BN.^[35–37] For example, the conductivity of nanoribbons became increased due to doping-like conducting edge states and vacancy defects.^[35] Line defects may create two deep narrow bands in a band gap which transformed h-BN from insulator to semiconductor.^[36] Although the high-resolution transmission electron microscopy (presented in the previous work)^[22] has shown the high crystalline quality of the h-BN sample, very few defects can still be observed. The inevitable defects may have a certain impact on the electrical properties of the single and double-layer BN, which is required for more in-depth research.

The ability to regulate the electronic characteristic of 2D materials plays a key role in the application in electronic and optoelectronic devices. The electronic characteristic can be tuned via various methods such as employing an electric field, mechanical strain, and varying thickness.^[38–40] Here, the influence of the load force on the electric properties of h-BN was studied. As shown in the I – V curves of monolayer h-BN (Figure 3a), the electron transport became much easier when the load force increased. And the diode feature was also weakened with the increased load force. The modulated electrical

characteristics may be due to the reduction of Schottky barrier height caused by increased strain.^[39,40] As to the bilayer h-BN, it was not so sensitive as monolayer h-BN to the load force. As illustrated in Figure 3b, no current was observed in I – V curves of bilayer h-BN when a weak load force was applied. When the load force was increased to a certain degree (≈ 88 nN), the current was suddenly observed in the negative voltage region. And it exhibited an obvious diode feature. Then, when the load force continued to increase, the I – V curve did not change significantly. This may be due to the excellent insulation of bilayer h-BN and the contact area of the tip and samples which need enough load force for the electron transport. Besides, the increased load force may decrease the interlayer distance which result in a weakened interlayer coupling resistance.^[40,41]

The I – V curves were obtained at the static measurement. To gain an insight into the dynamics of the force effect, current mappings were obtained by C-AFM under a fixed external bias and various load forces with different h-BN samples (Figures 4 and 5; Figures S4–S8, Supporting Information). As illustrated in current mappings, the current signal increased gradually with the increased load force when a positive or negative bias was applied. This phenomenon was consistent with the characteristics measured by I – V curves. More detailed information of the current signal can be obtained from the line-scan profiles of the current mappings under different load force (Figure S4, Supporting Information) marked with olive lines in Figure 4a. Moreover, in order to have a more intuitive understanding of the distribution of the current signal in the current mapping, the statistical distributions (Figures 4b and 5b) which exhibited a most probable current signal peak were summed up. Since the h-BN layers were not regular squares, we only selected a part region of the BN layer for statistical analysis of the current when different loading forces were applied. For monolayer, the corresponding raw data used for statistics was extracted from the region marked by the red square in Figure 4a, while for bilayer, the corresponding raw data was extracted from the region marked by the olive square in Figure 4a. For example, the most probable current signal of the selected monolayer h-BN zone was 2.17 ± 0.101 nA at the load force of 110 nN for monolayer h-BN when a positive bias was applied. As illustrated in the statistical distributions of the current signal for various load forces, the most probable current signal peak of the monolayer h-BN region under different load force maintained on the order of nA (Figures 4b and 5b). While for the bilayer h-BN region, the most probable current signal peak under different load forces only maintained

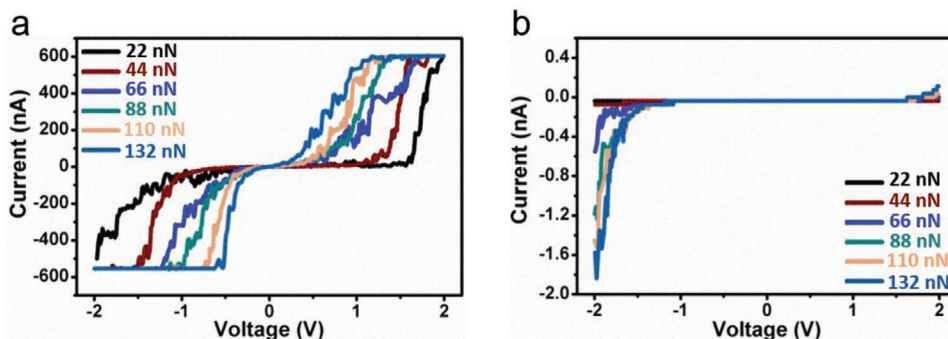


Figure 3. I – V curves under different applied load forces for a) monolayer h-BN and b) bilayer h-BN.

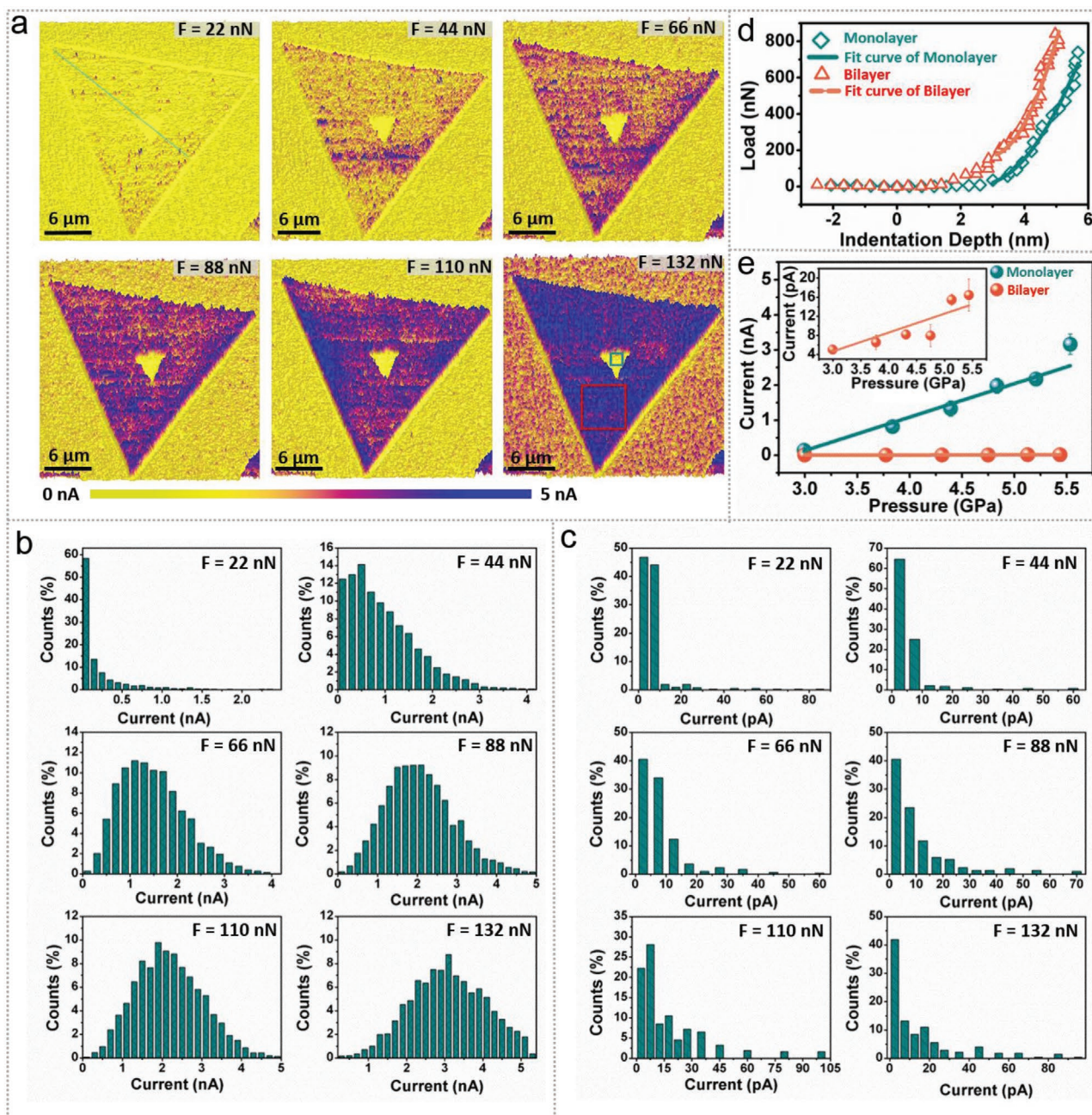


Figure 4. Force dependent current signal for both monolayer and bilayer h-BN zones when a positive external bias of +1.3 V was applied. a) C-AFM current mappings under different load forces. b) The corresponding statistics of the current signal under a series of load forces for the monolayer h-BN zone in Figure 4a (The corresponding raw data used for statistics was extracted from the monolayer zone marked by red square box in Figure 4a). c) The corresponding statistics of the current signal under a series of load forces for the bilayer h-BN zone in Figure 4a (The corresponding raw data used for statistics was extracted from the bilayer zone marked by olive square box in Figure 4a). d) Measured force–indentation curves of h-BN. By fitting the curves, the average elastic modulus of h-BN with monolayer and bilayer was obtained. e) Corresponding average current mappings under different pressure for the h-BN of the monolayer zone and bilayer zone. The average value of current for monolayer h-BN was calculated by randomly selecting three $6 \times 6 \mu\text{m}$ areas of the monolayer zones. And, the average value of current for bilayer h-BN was calculated by randomly selecting three $1 \times 1 \mu\text{m}$ areas of the bilayer zones.

on the order of pA (Figures 4c and 5c). Moreover, the most probable current signal peak of the monolayer h-BN region increased with the increased load force, while such discernible change of the current signal was not observed for the bilayer h-BN region (Figures 4b,c and 5b,c). It was consistent with the change of I – V

curves (Figure 3a,b) which showed monolayer h-BN was more sensitive to the load force. However, compared to the static electrical characteristic measurement, the current signal was much lower measured by dynamics scanning. It was possibly caused by localized changes in contact during dynamic scanning,^[42]

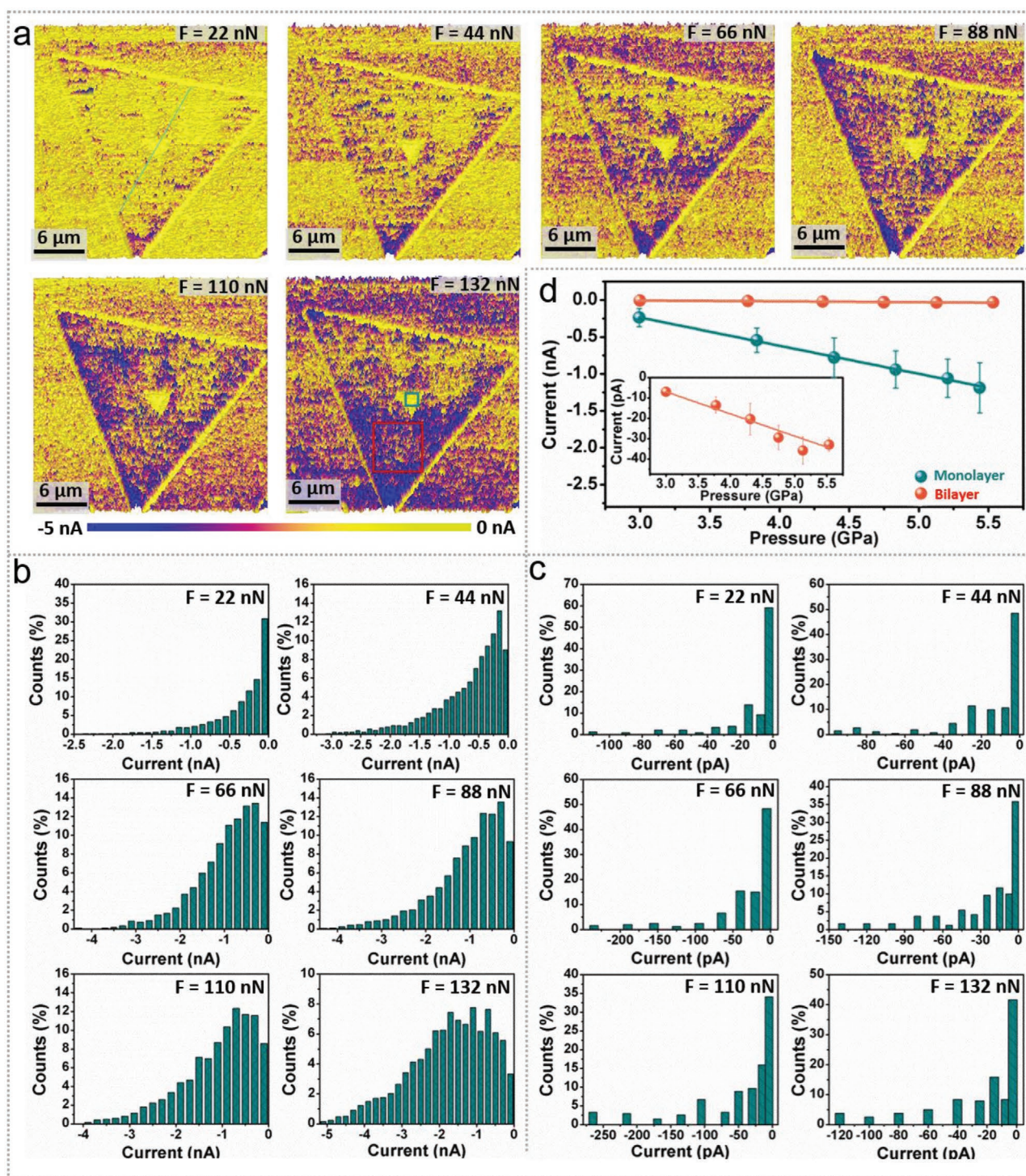


Figure 5. Force-dependent current signal for both monolayer and bilayer h-BN zones, when a negative external bias of -1.3 V was applied. a) C-AFM current mappings under different load forces. b) The corresponding statistics of the current signal under a series of load forces for the monolayer h-BN zone in Figure 5a (The corresponding raw data used for statistics was extracted from the bilayer zone marked by red square box in Figure 5a). c) The corresponding statistics of the current signal under a series of load forces for the bilayer h-BN zone in Figure 5a (The corresponding raw data used for statistics was extracted from the bilayer zone marked by olive square box in Figure 5a). d) Corresponding average current of current mappings under different pressure for the h-BN of the monolayer zone and bilayer zone. The average value of current for monolayer h-BN was calculated by randomly selecting three $6 \times 6 \mu\text{m}$ areas of the monolayer zone. And, the average value of current for bilayer h-BN was calculated by randomly selecting three $1 \times 1 \mu\text{m}$ areas of the bilayer zone.

which can be further improved in the future through design adjustment. Furthermore, dynamic scanning measurements can offer a high-speed response and statistical data of thousands of pixels which can eliminate the issues caused by artificiality.

To reveal the effect of pressure on the electrical characteristic, an effective electrical contact area was proposed during the C-AFM measurement because of the special tip geometry. The effective contact area can be approximated by the Hertz model:^[43]

$$A = \pi \left(\frac{RF}{K} \right)^{\frac{2}{3}} \quad (1)$$

Here, A represents the effective contact area. F stands for the load force. The R is the radius of the AFM tip used as 25 nm. K denotes the reduced Young's modulus which is calculated by:

$$\frac{1}{K} = \frac{3}{4} \left(\frac{1-\nu_s^2}{E_s} + \frac{1-\nu_t^2}{E_t} \right) \quad (2)$$

Here E_t is Young's module of the tip, ν_t and ν_s represent the Poisson ratios of the tip and h-BN sample, respectively. Here, $E_t = 165$ GPa, $\nu_t = 0.22$, and $\nu_s = 0.211$.^[26,44,45] E_s is Young's modulus of the h-BN which can be approximated by Hertz–Sneddon^[46]

$$F = \frac{2}{\pi} \frac{E}{1-\nu^2} \tan \alpha \delta^2 \quad (3)$$

where, α is the half opening angle of the indenting cone, used as 18°, and δ is the indentation of the sample under load force.

As illustrated in Figure 4d, load-indentation curves of monolayer h-BN and bilayer h-BN were obtained using AFM. The Young's modulus of h-BN with monolayer and bilayer could be deduced by fitting the loading curves using Equation (3). The Young's modulus of monolayer h-BN and bilayer h-BN were ≈ 355 and 328 GPa, respectively. These values were on the same order of magnitude as those obtained by previous studies using AFM.^[47–49] And, the value of Young's modulus of monolayer h-BN was much closer to that of bilayer h-BN which was consistent with the previous work.^[26] It suggested that the mechanical strength of BN nanosheets was insensitive to thickness. The relationship of the average value of current with the pressure was investigated (Figures 4e and 5d; Figures S5–S8, Supporting Information). The average value of current for monolayer BN was calculated by random selecting three $6 \times 6 \mu\text{m}$ areas of the monolayer zones, while the average value of current for bilayer BN was calculated by randomly selecting three $1 \times 1 \mu\text{m}$ areas of the bilayer zones. It was shown that when a positive bias was applied, the average value of current for monolayer h-BN linearly increased with the increased pressure with a slope of $0.9527 \text{ nA} \pm 0.0596 \text{ nA GPa}^{-1}$, and a correlation coefficient of 0.98 (Figure 4e). While, the average value of current for bilayer h-BN also linearly increased with the increased pressure, but with a much smaller slope of $0.0039 \text{ nA} \pm 0.0008 \text{ nA GPa}^{-1}$, and a lower correlation coefficient of 0.80. A similar phenomenon was also observed when a negative bias was applied (Figure 5d; Figures S6 and S8, Supporting

Information) which verified that monolayer h-BN was more sensitive to the load force. And this may offer a whole new pathway to tune the electrical characteristics of the electronic and optoelectronic devices based on h-BN.

3. Conclusion

In summary, based on the C-AFM technology, we investigated the different electrical properties of monolayer h-BN and bilayer h-BN. We found that bilayer h-BN showed quite different electrical characteristics from monolayer h-BN. We proposed that the difference of work functions between monolayer h-BN and bilayer h-BN contributed to the dissimilar electrical characteristics. Meanwhile, the interlayer coupling resistance due to coupling between the h-BN layers also made a great effect on the electron transport. Besides, the effect of load force for the electrical characteristics of h-BN with different layers was also investigated. It was found that the monolayer h-BN showed much more sensitivity to the load force than bilayer h-BN which may offer a new pathway to tune the electrical characteristics of multifunctional h-BN-based nano-electronic devices. This work provided very meaningful experimental data and a new sight to understand the role of the number of layers on electrical properties of h-BN, which we hope can offer meaningful suggestions for future studies and applications on h-BN and other 2D nanomaterials in general.

4. Experimental Section

Device Fabrication: Under a mixed gas of Ar and H₂ (500 sccm Ar, 10 sccm H₂), the Cu foil was first annealed at 1000 °C for 30 min at atmospheric pressure. Then, the precursor of ammonia borane was heated to 65 °C at the upstream of the tube in the sublimation process. The system was naturally cooled to room temperature after the growth time of ≈ 1 h. The obtained h-BN samples with an area of 1.5×1.5 cm were fixed on ITO glasses. The sample was connected to the ground through an external circuit from the Cu substrate.

Characterization and Measurements: The h-BN samples were investigated by a field-emission SEM (Hitachi, SU8020). All AFM mappings were obtained by using the equipment Dimension Icon (Bruker, USA) with the conductive tips coated Pt/Ir (EFM, NanoWorld; the spring constant radii of the tips were 2.8 N m⁻¹ and 25 nm, respectively). The current mappings were obtained in the conductive atomic force microscopy (C-AFM) mode. And, the potential mappings were obtained in kelvin probe force microscopy (KPFM) mode. The work function of the Pt/Ir tip was ≈ 4.75 eV, which was calibrated using a standard sample HOPG. Besides, all the AFM experiments were measured in a glove box that was filled with dried nitrogen.

Supporting Information

Supporting Information is available from the Wiley Online Library or from the author.

Acknowledgements

N.W. and Y.S. contributed equally to this work. This work was supported by the National Key R&D Project from the Minister of Science and

Technology in China (No. 2016YFA0202701), the University of Chinese Academy of Sciences (Grant No. Y8540XX2D2), and the National Natural Science Foundation of China (No. 52072041, No. 52025023, and No. 52021006).

Conflict of Interest

The authors declare no conflict of interest.

Data Availability Statement

Research data are not shared.

Keywords

atomic force microscope (AFM), different layers of 2D materials, electrical properties, hexagonal boron nitride (h-BN)

Received: March 19, 2021

Revised: June 15, 2021

Published online: July 26, 2021

- [1] K. Watanabe, T. Taniguchi, H. Kanda, *Nat. Mater.* **2004**, *3*, 404.
- [2] Y. Kubota, K. Watanabe, O. Tsuda, T. Taniguchi, *Science* **2007**, *317*, 932.
- [3] J. G. Kho, K. T. Moon, J. H. Kim, D. P. Kim, *J. Am. Ceram. Soc.* **2000**, *83*, 2681.
- [4] K. K. Kim, A. Hsu, X. Jia, S. M. Kim, Y. Shi, M. Hofmann, D. Nezich, J. F. Rodriguez-Nieva, M. Dresselhaus, T. Palacios, J. Kong, *Nano Lett.* **2012**, *12*, 161.
- [5] L. Liu, Y. P. Feng, Z. X. Shen, *Phys. Rev. B* **2003**, *68*, 104102.
- [6] D. Usachov, A. Fedorov, O. Vilkov, V. K. Adamchuk, L. V. Yashina, L. Bondarenko, A. A. Saranin, A. Gruneis, D. V. Vyalikh, *Phys. Rev. B* **2012**, *86*, 155151.
- [7] H. Henck, D. Pierucci, G. Fugallo, J. Avila, G. Cassabois, Y. J. Dappe, M. G. Silly, C. Chen, B. Gil, M. Gatti, F. Sottile, F. Sirotti, M. C. Asensio, A. Ouerghi, *Phys. Rev. B* **2017**, *95*, 085410.
- [8] R. J. Koch, J. Katoch, S. Moser, D. Schwarz, R. K. Kawakami, A. Bostwick, E. Rotenberg, C. Jozwiak, S. Ulstrup, *Phys. Rev. Mater.* **2018**, *2*, 074006.
- [9] R. Haubner, M. Wilhelm, R. Weissenbacher, B. Lux, in *High Performance Non-Oxide Ceramics II*, Vol. 102 (Ed: M. Jansen), Structure and Bonding, Springer, Berlin **2002**, p. 1.
- [10] K. K. Kim, S. M. Kim, Y. H. Lee, *J. Korean Phys. Soc.* **2014**, *64*, 1605.
- [11] W. Yang, G. Chen, Z. Shi, C.-C. Liu, L. Zhang, G. Xie, M. Cheng, D. Wang, R. Yang, D. Shi, K. Watanabe, T. Taniguchi, Y. Yao, Y. Zhang, G. Zhang, *Nat. Mater.* **2013**, *12*, 792.
- [12] D. Chen, R. Qiao, X. Xu, W. Dong, L. Wang, R. Ma, C. Liu, Z. Zhang, M. Wu, L. Liu, L. Bao, H.-T. Wang, P. Gao, K. Liu, D. Yu, *Nanoscale* **2019**, *11*, 4226.
- [13] L. Britnell, R. V. Gorbachev, R. Jalil, B. D. Belle, F. Schedin, A. Mishchenko, T. Georgiou, M. I. Katsnelson, L. Eaves, S. V. Morozov, N. M. R. Peres, J. Leist, A. K. Geim, K. S. Novoselov, L. A. Ponomarenko, *Science* **2012**, *335*, 947.
- [14] L. Britnell, R. V. Gorbachev, A. K. Geim, L. A. Ponomarenko, A. Mishchenko, M. T. Greenaway, T. M. Fromhold, K. S. Novoselov, L. Eaves, *Nat. Commun.* **2013**, *4*, 1794.
- [15] D. Liu, X. Chen, Y. Yan, Z. Zhang, Z. Jin, K. Yi, C. Zhang, Y. Zheng, Y. Wang, J. Yang, X. Xu, J. Chen, Y. Lu, D. Wei, A. T. S. Wee, D. Wei, *Nat. Commun.* **2019**, *10*, 1188.
- [16] L. Wang, B. Wu, H. Liu, L. Huang, Y. Li, X. Chen, P. Peng, L. Fu, Y. Yang, P. Hu, Y. Liu, *Mater. Chem. Front.* **2017**, *1*, 1836.
- [17] Z. Liu, L. Ma, G. Shi, W. Zhou, Y. Gong, S. Lei, X. Yang, J. Zhang, J. Yu, K. P. Hackenberg, A. Babakhani, J.-C. Idrobo, R. Vajtai, J. Lou, P. M. Ajayan, *Nat. Nanotechnol.* **2013**, *8*, 119.
- [18] L. Liu, J. Park, D. A. Siegel, K. F. McCarty, K. W. Clark, W. Deng, L. Basile, J. C. Idrobo, A.-P. Li, G. Gu, *Science* **2014**, *343*, 163.
- [19] S. M. Kim, A. Hsu, M. H. Park, S. H. Chae, S. J. Yun, J. S. Lee, D.-H. Cho, W. Fang, C. Lee, T. Palacios, M. Dresselhaus, K. K. Kim, Y. H. Lee, J. Kong, *Nat. Commun.* **2015**, *6*, 9662.
- [20] J. Li, Y. Li, J. Yin, X. Ren, X. Liu, C. Jin, W. Guo, *Small* **2016**, *12*, 3645.
- [21] G. Lu, T. Wu, Q. Yuan, H. Wang, H. Wang, F. Ding, X. Xie, M. Jiang, *Nat. Commun.* **2015**, *6*, 6160.
- [22] L. Wang, X. Xu, L. Zhang, R. Qiao, M. Wu, Z. Wang, S. Zhang, J. Liang, Z. Zhang, Z. Zhang, W. Chen, X. Xie, J. Zong, Y. Shan, Y. Guo, M. Willinger, H. Wu, Q. Li, W. Wang, P. Gao, S. Wu, Y. Zhang, Y. Jiang, D. Yu, E. Wang, X. Bai, Z.-J. Wang, F. Ding, K. Liu, *Nature* **2019**, *570*, 91.
- [23] X. Wei, Z. Meng, L. Ruiz, W. Xia, C. Lee, J. W. Kysar, J. C. Hone, S. Keten, H. D. Espinosa, *ACS Nano* **2016**, *10*, 1820.
- [24] A. Castellanos-Gomez, M. Poot, G. A. Steele, H. S. J. van der Zant, N. Agrait, G. Rubio-Bollinger, *Adv. Mater.* **2012**, *24*, 772.
- [25] J. Tao, W. Shen, S. Wu, L. Liu, Z. Feng, C. Wang, C. Hu, P. Yao, H. Zhang, W. Pang, X. Duan, J. Liu, C. Zhou, D. Zhang, *ACS Nano* **2015**, *9*, 11362.
- [26] A. Falin, Q. Cai, E. J. G. Santos, D. Scullion, D. Qian, R. Zhang, Z. Yang, S. Huang, K. Watanabe, T. Taniguchi, M. R. Barnett, Y. Chen, R. S. Ruoff, L. H. Li, *Nat. Commun.* **2017**, *8*, 15815.
- [27] L. Britnell, R. V. Gorbachev, R. Jalil, B. D. Belle, F. Schedin, M. I. Katsnelson, L. Eaves, S. V. Morozov, A. S. Mayorov, N. M. R. Peres, A. H. Castro Neto, J. Leist, A. K. Geim, L. A. Ponomarenko, K. S. Novoselov, *Nano Lett.* **2012**, *12*, 1707.
- [28] M. Piquemal-Banci, R. Galceran, S. Caneva, M.-B. Martin, R. S. Weatherup, P. R. Kidambi, K. Bouzheouane, S. Xavier, A. Anane, F. Petroff, A. Fert, J. Robertson, S. Hofmann, B. Dlubak, P. Seneorl, *Appl. Phys. Lett.* **2016**, *108*, 102404.
- [29] F. Guinea, *Phys. Rev. B* **2007**, *75*, 235433.
- [30] J. Kwon, A. Prakash, S. R. Das, D. B. Janes, *Phys. Rev. Appl.* **2018**, *10*, 064029.
- [31] S. Das, J. Appenzeller, *Phys. Status Solidi-RRL* **2013**, *7*, 268.
- [32] A. V. Bruce, S. Liu, J. N. Fry, H.-P. Cheng, *Phys. Rev. B* **2020**, *102*, 115415.
- [33] J. Kwon, C. J. Delker, C. T. Harris, S. R. Das, D. B. Janes, *J. Appl. Phys.* **2020**, *128*, 094501.
- [34] Y. Sui, J. Appenzeller, *Nano Lett.* **2009**, *9*, 2973.
- [35] H. B. Zeng, C. Y. Zhi, Z. H. Zhang, X. L. Wei, X. B. Wang, W. L. Guo, Y. Bando, D. Golberg, *Nano Lett.* **2010**, *10*, 5049.
- [36] X. Jianga, L. H. X. Zuoa, Q. G. H. Lia, X. Lic, X. Zhenga, X. Jiangb, B. Cuia, D. Lia, D. Liua, F. Qu, *Comput. Mater. Sci.* **2020**, *183*, 109799.
- [37] O. L. Krivanek, M. F. Chisholm, V. Nicolosi, T. J. Pennycook, G. J. Corbin, N. M. Dellby, F. Murfitt, C. S. Own CS, Z. S. Szilagy, M. P. Oxley, S. T. Pantelides, S. J. Pennycook, *Nature* **2010**, *464*, 571.
- [38] A. Bafekry, C. Nguyen, M. M. Obeid, M. Ghergherehchi, *New J. Chem.* **2020**, *44*, 15785.
- [39] S. An, S. Wu, C. S. Tan, G.-E. Chang, X. Gong, M. Kim, *J. Mater. Chem. C* **2020**, *8*, 13557.
- [40] M. H. Liao, P. S. Kuo, S. R. Jan, S. T. Chang, C. W. Liu, *Appl. Phys. Lett.* **2006**, *88*, 143509.
- [41] A. Bafekry, M. Yagmurcukardes, M. Shahrokhi, M. Ghergherehchi, *Carbon* **2020**, *168*, 220.

- [42] L. Wang, S. Liu, X. Feng, C. Zhang, L. Zhu, J. Zhai, Y. Qin, Z. L. Wang, *Nat. Nanotechnol.* **2020**, *15*, 661.
- [43] J. Y. Park, M. Salmeron, *Chem. Rev.* **2014**, *114*, 677.
- [44] J. Liu, A. Goswami, K. Jiang, F. Khan, S. Kim, R. McGee, Z. Li, Z. Hu, J. Lee, T. Thundat, *Nat. Nanotechnol.* **2018**, *13*, 112.
- [45] Q. Peng, W. Ji, S. De, *Comp. Mater. Sci.* **2012**, *56*, 11.
- [46] J. Domke, M. Radmacher, *Langmuir* **1998**, *14*, 3320.
- [47] L. Song, L. J. Ci, H. Lu, P. B. Sorokin, C. H. Jin, J. Ni, A. G. Kvashnin, D. G. Kvashnin, J. Lou, B. I. Yakobson, P. M. Ajayan, *Nano Lett.* **2010**, *10*, 3209.
- [48] J. T. Wu, B. L. Wang, Y. J. Wei, R. G. Yang, M. Dresselhaus, *Mater. Res. Lett.* **2013**, *1*, 200.
- [49] M. Mirnezhad, R. Ansari, H. Rouhi, *Superlattices Microstruct.* **2013**, *53*, 223.